

A NEW LOOK AT LOW-RANK RECURRENT NEURAL NETWORKS

Anonymous authors

Paper under double-blind review

ABSTRACT

Low-rank recurrent neural networks (RNNs) have recently gained prominence as a framework for understanding how neural systems solve complex cognitive tasks. However, training and interpreting these networks remains an important open problem. Here we address these challenges by adopting a view of low-rank RNNs as parametrizing a low-dimensional ordinary differential equation (ODE) using a set of nonlinear basis functions. This perspective, which arises from an approach known as the “neural engineering framework”, reveals that low-rank RNNs are equivalent to neural ODEs with a single hidden layer. We show that training a low-rank RNN to implement a particular dynamical system can thus be formalized as least-squares regression in a random basis. This allows us to propose a new method for finding the smallest RNN capable of implementing a dynamical system using a variant of orthogonal matching pursuit. More generally, our perspective clarifies limits on the expressivity of low-rank RNNs, such as the fact that without inputs, a low-rank RNN with sigmoidal nonlinearity can only implement odd-symmetric functions. We delve further into the role of inputs in shaping network dynamics and show that RNNs can produce identical trajectories using a wide variety of static or time-varying dynamics; this highlights the importance of perturbations for inferring dynamics from observed neural trajectories. Finally, we highlight the usefulness of our framework by comparing to RNNs trained using backprop-through-time on neuroscience-inspired tasks, showcasing that our method achieves faster and more accurate learning with smaller networks than gradient-based training.

1 INTRODUCTION

Recurrent neural networks (RNNs) provide a popular tool for analyzing the computational capabilities of neural populations and the mechanisms that enable them to carry out complex cognitive tasks (Miller et al., 2003; Barak, 2017; Mastrogiuseppe & Ostojic, 2018; Schaeffer et al., 2020; Duncker & Sahani, 2021; Dubreuil et al., 2022). A substantial literature focuses on “goal-driven” or “task-driven” approaches in which an RNN is trained to perform a particular cognitive task of interest, and then analyzed to determine what dynamics it uses to solve the task (Mante et al., (2013); Sussillo (2014); Kanitscheider & Fiete (2017); Pollock & Jazayeri (2020); Turner et al. (2021)). However, both the training and the interpretation of such networks are noteworthy problems of interest.

A wide variety of methods have been proposed for training RNNs on cognitive tasks, including: (1) reservoir computing methods, in which a fixed set of random recurrent weights generate a high-dimensional nonlinear dynamics, and training is applied only to output weights (Jaeger 2001; Maass et al., 2002); (2) FORCE training, in which a set of random recurrent weights are adjusted using iterative low-rank updates via recursive least-squares (Sussillo & Abbott (2009); DePasquale et al. (2018); and (3) methods that adjust all recurrent weights using deep-learning inspired approaches such as back-propagation-through-time (BPTT) (Pearlmutter (1990); Sussillo & Barak (2013); Lillicrap & Santoro (2019)). Although recent literature has focused primarily on this latter class of gradient-based training methods, they nevertheless face a variety of challenges, including high computational cost, sensitivity to initialization and hyper-parameters (e.g., learning rate, network size), and susceptibility to vanishing and exploding gradients (Lukoševičius & Jaeger 2009; Schuessler et al., 2020; Langdon & Engel, 2022; Liu et al., 2023).

054 Even once they are trained (via any of the above methods), interpreting RNNs to gain insight
 055 into task performance remains challenging. Common approaches tend to rely on finding fixed or
 056 “slow” points and then using dimensionality reduction methods to visualize projected flow fields
 057 Sussillo & Barak (2013); Mante et al. (2013). However, fixed-point finding algorithms are difficult to
 058 apply to high-dimensional systems, and it often unclear how accurately low-D projections reflect a
 059 network’s true dynamics. Previous work has shown that task-trained RNNs with similar performance
 060 can nevertheless exhibit different dynamics, raising the question of whether their solutions reveal
 061 universal features of task computations (Barak 2017; Williams et al. 2021).

062 One recent advance that overcomes or alleviates many of these difficulties is a theory of low-rank
 063 RNNs (Mastrogiuseppe & Ostojic 2018; Beiran et al. 2021; Dubreuil et al. 2022; Valente et al.
 064 2022). Rather than training a high-dimensional network and then attempting to visualize its behavior
 065 using low-D projections, this literature has shown that a wide variety of tasks can be implemented
 066 directly in RNNs with intrinsically low dimension, where the dimensionality is set by the rank of the
 067 recurrent weight matrix plus input dimensions.

068 A parallel arm of research has focused on developing methods to embed low-dimensional quantities
 069 into high-dimensional network activity (Eliasmith & Anderson 2003; Stewart 2012; Abbott et al.
 070 2016; Boerlin et al. 2013; Alemi et al. 2018). Of particular relevance to our work is the Neural
 071 Engineering Framework (NEF), which formalizes encoding a stimulus into neuron action potentials
 072 using basis functions, and learning an appropriate linear decoder via regression. While NEF has been
 073 widely explored, we are not aware of prior work explicitly describing non-linear recurrent dynamics
 074 in NEF networks as low-rank RNNs. Additionally, while Beiran et al. (2021) use such a regression
 075 framework, there is no interpretational geometric insight through the use of basis functions.

076 In this work, we propose an alternate RNN training strategy that is deterministic, requires low
 077 compute time while also addressing interpretability issues of such models. First, we use NEF to
 078 provide an alternate view of low-rank RNNs. Specifically, we develop flexible representations
 079 through the construction of a randomized basis spanned by the low-dimensional dynamical system.
 080 These basis functions are used as regressors to embed a target non-linear ODE in the low-rank
 081 RNN using least-squares regression, thereby overcoming issues of gradient-based training. Second,
 082 using this framework we provide empirical and theoretical evidence regarding the representational
 083 limits of low-rank RNNs. In particular, we emphasize the necessity of neuron-specific inputs for
 084 embedding odd-symmetric dynamics. Third, using a variant of orthogonal matching pursuit we derive
 085 the smallest RNN that can implement any target ODE. Fourth, we offer novel insights on the
 086 influence of *time-varying* inputs in embedding both autonomous and non-autonomous ODEs. Using
 087 this, we provide empirical evidence on how similar trajectories can arise from significantly different
 088 dynamical systems. Additionally, we utilize this finding to underscore the necessity of perturbations
 089 for differentiating between these systems. Lastly, we also apply our method to learn simulated ODEs
 090 which arise from a neuroscience binary decision making task, thereby proving the effectiveness of
 091 our method.

093 2 BACKGROUND: RECURRENT NEURAL NETWORKS (RNNs)

094
 095 Consider a population of d rate-based neurons, with membrane potentials $\mathbf{x} = [x_1, \dots, x_d]^\top$ and
 096 firing rates denoted by $\phi(\mathbf{x}) = [\phi(x_1), \dots, \phi(x_d)]^\top$, where $\phi(\cdot)$ is a scalar function mapping the
 097 membrane potential to firing rate (e.g., sigmoid, hyperbolic tangent, or ReLU). The dynamics of a
 098 generic RNN are given by the vector ordinary differential equation and a linear output:
 099

$$101 \quad \dot{\mathbf{x}} = -\mathbf{x} + J\phi(\mathbf{x}) + I\mathbf{u}(t) \tag{1}$$

$$102 \quad \mathbf{z} = W\phi(\mathbf{x}), \tag{2}$$

103
 104 where J is a $d \times d$ recurrent weight matrix, I is a $d \times d_{in}$ matrix of input weights, $\mathbf{u}(t)$ is a d_{in} -
 105 dimensional input signal, and $\dot{\mathbf{x}} = [\frac{dx_1}{dt}, \dots, \frac{dx_d}{dt}]^\top$ denotes the vector of time derivatives of \mathbf{x} . To
 106 describe behavioral outputs, the model contains a mapping from network activity to an output variable
 107 \mathbf{z} : where W denotes a $d_{out} \times d$ matrix of readout weights.

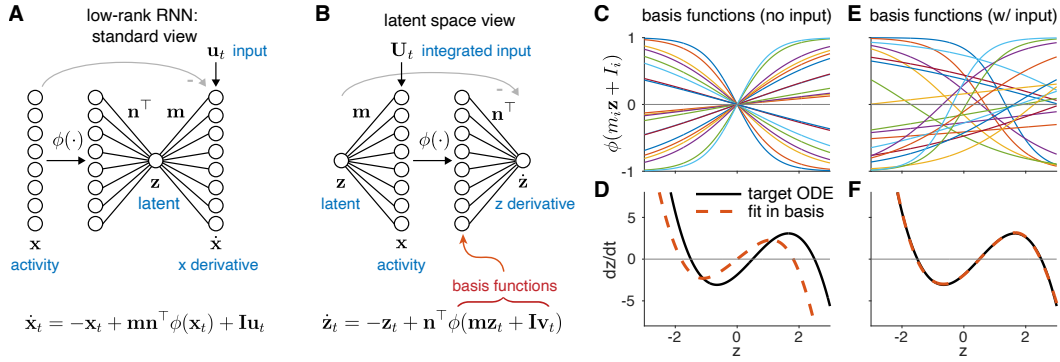


Figure 1: Two equivalent views of low-rank RNNs. (A) Standard view of rank-1 RNN with 8 neurons \mathbf{x} and 1 latent dimension \mathbf{z} . (B) Alternate view of the same network, now framed in terms of the dynamics of latent \mathbf{z} . This shows that a low-rank RNN is equivalent to a neural ODE with a single hidden layer (Chen et al., 2018). (C) Basis functions obtained by sampling slope parameters $m_i \sim \mathcal{N}(0, 1)$, but without input ($\mathbf{v}_t = 0$). (D) Attempting to fit an example ODE using this basis recovers only the odd-symmetric component, since all basis functions are odd symmetric. (E) Adding inputs allows basis functions have random horizontal offsets. Here we sampled the input weights $I_i \sim \mathcal{N}(0, 1)$ and set input $\mathbf{v}_t = 1$. (Note that this could also be obtained by using per-neuron “biases”). (F) Least squares fitting of \mathbf{n} using the basis from (E) provides good fit to the target ODE.

2.1 LOW-RANK RNNs

This network model described above becomes a *low-rank RNN* if the recurrent weight matrix J has reduced rank $r < d$, which implies it can be factorized as:

$$J = MN^\top = \sum_{i=1}^r \mathbf{m}_i \mathbf{n}_i^\top. \quad (3)$$

Here \mathbf{m}_i and \mathbf{n}_i represent the columns of the $d \times r$ matrices M and N , respectively. In this case, the state vector $\mathbf{x}(t)$ will evolve in a subspace of at most $r + d_{in}$ dimensions (Mastrogiuseppe & Ostojic 2018; Dubreuil et al., 2022). Activity in the remaining dimensions will decay to zero due to the decay term ($-\mathbf{x}$) in (eq. 1).

In this setting, the network state \mathbf{x} can be re-written as

$$\mathbf{x}(t) = M\boldsymbol{\kappa}(t) + I\mathbf{v}(t), \quad (4)$$

where $\boldsymbol{\kappa}$ is a so-called “latent” vector representing activity in the r -dimensional recurrent subspace, and $\mathbf{v}(t)$ represents the low-pass filtered input signals $\mathbf{u}(t)$ (Dubreuil et al., 2022; Valente et al., 2022). Finally, the low-dimensional recurrent dynamics can be represented in terms of a differential equation: $\dot{\boldsymbol{\kappa}} = F(\boldsymbol{\kappa}, \mathbf{u})$, where F is a nonlinear function of the latent state $\boldsymbol{\kappa}$ and input \mathbf{u} .

3 AN ALTERNATE VIEW OF LOW-RANK RNNs

In the framework described above, training a low-rank RNN to produce a desired output $\mathbf{z}(t)$ from an input $\mathbf{u}(t)$ requires learning the model parameters $\{N, M, I, W\}$, which is typically carried out using back-propagation through time (Valente et al., 2022). Here we describe a different approach to low-rank RNNs, which greatly simplifies this training procedure and provides a more intuitive portrait of the network’s dynamical capabilities.

We begin by considering the problem of embedding an arbitrary low-dimensional dynamical system into a low-rank RNN. Specifically, suppose we wish to set the model parameters so that \mathbf{z} obeys the dynamics of an particular nonlinear ODE:

$$\dot{\mathbf{z}} = g(\mathbf{z}), \quad (5)$$

for some function g . We will then identify this output with the latent vector defining the network’s activity in the recurrent subspace: $\mathbf{z}(t) \triangleq \boldsymbol{\kappa}(t)$. This implies that the dimensionality of the output is

equal to the rank of the network, $r = d_{out}$, and constrains the output weights to be the projection operator onto the column space of M , that is, $W = M(M^\top M)^{-1}$. We are then left with the problem of setting the weights M , N , and I so that the latent vector, which we now refer to as $\mathbf{z}(t)$, evolves according to (eq. 5). (Note however the model output need match the dimensionality of the latent variable; in cases where desired output is lower-dimensional than \mathbf{z} , the output can be expressed as $\mathbf{z}' = A\mathbf{z}$, where A is some fixed matrix of output weights that, for example, selects only one component of \mathbf{z} .)

For simplicity, we begin with the case of a scalar \mathbf{z} . This corresponds to an RNN with rank-1 recurrent weight matrix $J = \mathbf{m}\mathbf{n}^\top$, which is simply an outer product of weight vectors \mathbf{m} and \mathbf{n} . Assume that the input is also scalar, and that the input vector I is orthogonal to \mathbf{m} (although we can relax this constraint later). Following previous work (Beiran et al. 2021, Dubreuil et al. 2022, Valente et al. 2022) (eq. 4), the network state can be decomposed as a time-varying linear combination of \mathbf{m} and I :

$$\mathbf{x}(t) = \mathbf{m}\mathbf{z}(t) + I\mathbf{v}(t), \quad (6)$$

where $\mathbf{v}(t)$ represents the low-pass filtered input, resulting from the linear dynamical system $\dot{\mathbf{v}} = -\mathbf{v} + \mathbf{u}(t)$. The fact that \mathbf{m} and I are orthogonal means that we can write the dynamics governing the latent variable explicitly as:

$$\dot{\mathbf{z}} = -\mathbf{z} + \mathbf{n}^\top \phi(\mathbf{m}\mathbf{z} + I\mathbf{v}(t)) \quad (7)$$

a result shown previously in Valente et al. (2022), and which is schematized in Fig. 1. Given this expression, our goal of embedding an arbitrary ODE $\dot{\mathbf{z}} = g(\mathbf{z})$ into the network can be viewed as setting the model parameters so that

$$g(\mathbf{z}) + \mathbf{z} \approx \mathbf{n}^\top \phi(\mathbf{m}\mathbf{z} + I\mathbf{v}(t)) \quad (8)$$

To achieve this, note that the right-hand-side can be viewed as a linear combination of terms $\phi(m_i\mathbf{z} + I_i\mathbf{v}(t))$ with weights n_i , for $i \in \{1, \dots, d\}$. Each of these terms can be viewed as a basis function in \mathbf{z} for representing the target $g(\mathbf{z}) + \mathbf{z}$. More specifically, if ϕ is the hyperbolic tangent function, each such term is a shifted, scaled tanh function in \mathbf{z} , where m_i is the slope and $I_i\mathbf{v}(t)$ is the offset. This means that we can view the problem of embedding $g(\mathbf{z})$ into a low-rank RNN as the problem of setting \mathbf{m} and I to build an appropriate set of basis functions, and setting \mathbf{n} so that the linear combination of basis functions approximates $g(\mathbf{z}) + \mathbf{z}$. This approach formalizes the connection between low-rank RNNs and the NEF (Eliasmith & Anderson, 2003; Barak & Romani, 2021), and shows that a low-rank RNN corresponds to a neural ODE with a single hidden layer (Chen et al. 2018, Pellegrino et al. 2023, Pals et al. 2024).

Already, this perspective makes an important limitation clear: if the inputs $\mathbf{v}(t)$ are zero, the basis functions are all odd-symmetric (that is, $g(m_i\mathbf{z}) = -g(-m_i\mathbf{z})$ for all \mathbf{z}), crossing the origin only at zero. (see Fig. 1C). Because $-\mathbf{z}$ is also odd-symmetric, and the linear combination of odd-symmetric functions is odd-symmetric, this means that in the absence of inputs, the network can only capture the odd-symmetric component of $g(\mathbf{z})$. A low-rank RNN is therefore not a universal approximator unless it has inputs, or equivalently, different biases or offsets to each neuron. If the ϕ is instead taken to be ReLu, the problem is even more severe: each basis function is a linear function with non-zero slope on either $\mathbf{z} > 0$ or $\mathbf{z} < 0$. Thus the network can only approximate $g(\mathbf{z})$ that are piecewise linear functions broken at the origin. (See SI Fig. SI-1).

If we set the filtered input to be the constant $\mathbf{v} = 1$, we see that the problem of embedding an arbitrary ODE in a low-rank RNN amounts to fitting the ODE in a basis of shifted and scaled basis functions in \mathbf{z} . To achieve this, we propose to sample the scales (elements of \mathbf{m}) and offsets (elements of I) to obtain a random basis, and then fit \mathbf{n} by least-squares regression, namely:

$$\hat{\mathbf{n}} = (\phi(\mathbf{z}_{grid}\mathbf{m}^\top + I^\top)^\top \phi(\mathbf{z}_{grid}\mathbf{m}^\top + I^\top))^{-1} \phi(\mathbf{z}_{grid}\mathbf{m}^\top + I^\top)^\top (g(\mathbf{z}_{grid}) + \mathbf{z}_{grid}), \quad (9)$$

where \mathbf{z}_{grid} denotes a grid of points at which we wish to fit $g(\mathbf{z})$. Note that we could use weighted least squares if we care more about accurately approximating certain regions of $g(\mathbf{z})$, or add a small ridge penalty if the design matrix (whose columns are given by the basis functions evaluated at \mathbf{z}_{grid}) is ill-conditioned.

Fig. 1 shows an illustration of this approach for an example ODE, here chosen to be a cubic polynomial with two stable fixed points and one unstable fixed point. Note that the network cannot approximate $g(\mathbf{z})$ when the inputs are set to zero (Fig. 1C-D), but can do so with near-perfect accuracy when both the \mathbf{m} vector and the (constant) inputs $I\mathbf{v}$ are drawn from a Gaussian distribution (Fig. 1E-F).

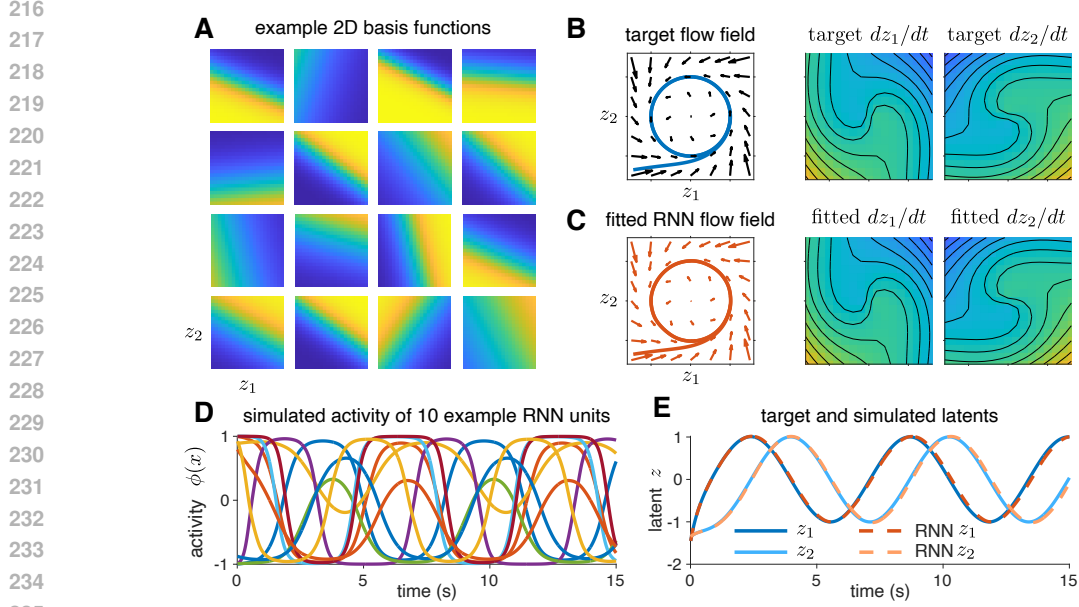


Figure 2: Embedding a 2-dimensional nonlinear ODE into a rank-2 RNN. **(A)** Example basis functions obtained by sampling M and I coefficients from a zero-mean Gaussian, producing randomly oriented, scaled, and shifted hyperbolic tangent functions. **(B)** A target two-dimensional nonlinear dynamical system, containing a stable limit cycle on a circle of radius one, represented as a flow field (left), or by its component functions $g_1(\mathbf{z}) = \frac{dz_1}{dt}$ and $g_2(\mathbf{z}) = \frac{dz_2}{dt}$ (right). **(C)** Least squares fitting of weight vectors \mathbf{n}_1 and \mathbf{n}_2 produces a near perfect match to the target flow field, and functions g_1 and g_2 . **(D)** Output firing rates $\phi(x_i)$ for 10 example units (i.e. $i \in \{1, \dots, 10\}$) during the red example trajectory shown in panel C. **(E)** Simulated trajectories from the true ODE (blue trace in panel B) and latent variable of the fitted RNN (red trace from panel C), plotted as a function of time, showing good agreement between the target ODE and the RNN output. Note that fitting was closed-form, and did not require backprop-through-time.

3.1 MULTI-DIMENSIONAL DYNAMICAL SYSTEMS

We can apply this same regression-based approach to higher-dimensional nonlinear dynamical systems, where $\text{rank } r = \dim(\mathbf{z}) > 1$. In two dimensions, the basis functions are given by $\phi(m_{1i}z_1 + m_{2i}z_2 + I_i)$, which are scaled, shifted tanh functions with a random orientation (see Fig. 2A). Approximating a 2D dynamical system with a rank-2 RNN can then be written as the problem of fitting two different nonlinear functions $g_1(\mathbf{z})$ and $g_2(\mathbf{z})$ using two different linear combinations of the same 2D basis functions:

$$g(\mathbf{z}) = \begin{bmatrix} g_1(\mathbf{z}) \\ g_2(\mathbf{z}) \end{bmatrix} \approx - \begin{bmatrix} z_1 \\ z_2 \end{bmatrix} + \begin{bmatrix} \mathbf{n}_1^\top \phi(M\mathbf{z} + I) \\ \mathbf{n}_2^\top \phi(M\mathbf{z} + I) \end{bmatrix}, \quad (10)$$

where $M = [\mathbf{m}_1 \mathbf{m}_2]$ is a $d \times 2$ matrix whose columns define the slope and orientation of each basis function, I is once again a column vector of offsets, and we have assumed constant input ($\mathbf{v} = 1$). Note once again that if we do not include inputs, the basis functions are all radially odd-symmetric around the origin. Thus, once again, the RNN will only be able to capture radially odd-symmetric $g(\mathbf{z})$, and is not a universal approximator unless we include nonzero offsets $I\mathbf{v} \neq 0$.

To embed a given multi-dimensional ODE $g(\mathbf{z})$ into a low-rank RNN, we once again generate a random basis by sampling the elements of $M \in \mathbb{R}^{d \times 2}$ and $I \in \mathbb{R}^d$ from a Gaussian distribution. The problem factorizes into learning each column vector \mathbf{n}_i for each dimension of the g , we have:

$$\hat{\mathbf{n}}_i = (\phi(Z_{grid}M^\top + I^\top)^\top \phi(Z_{grid}M^\top + I^\top))^{-1} \phi(Z_{grid}M^\top + I^\top)^\top (g(Z_{grid}) + Z_{grid}), \quad (11)$$

for $i = 1, 2$. This differs from the 1D case above only in that Z_{grid} is now a r -column matrix of grid points, where each row contains the coordinates of a single point in \mathbf{z} . Note that these grid

points need not be uniformly sampled; we could sample them from an arbitrary distribution, or use a collection of points from simulating the ODE from a variety of starting points.

Fig. 2 shows an application to an example 2-dimensional nonlinear ODE, in this case containing a stable limit cycle. Note that this 2D system is highly nonlinear and not radially odd-symmetric, so once again (Section A.2), embedding the system in a low-rank RNN fails if we do not include inputs (or per-neuron biases).

4 FINDING THE SMALLEST RNN FOR A GIVEN DYNAMICAL SYSTEM

We now turn to the question of finding the smallest RNN that can accurately implement a known nonlinear dynamical system, $g(\mathbf{z})$, focusing on a scalar z . In other words we aim to determine the minimum number of neurons ($d' \ll d$) needed by the network to approximate the function $g(\mathbf{z})$. Our goal is thus to solve an optimization problem that imposes a sparsity constraint on the dimensionality of our basis set $B(\mathbf{m}, I)$, while still solving for an appropriate linear weighting \mathbf{n} .

More formally, this implies selecting the best d' entries from $B(\mathbf{m}, I)$, to create a basis:

$$B_{d'}(\mathbf{m}, I) = \begin{bmatrix} \phi(m_{i_1} \mathbf{z} + I_{i_1}) \\ \phi(m_{i_2} \mathbf{z} + I_{i_2}) \\ \vdots \\ \phi(m_{i_{d'}} \mathbf{z} + I_{i_{d'}}) \end{bmatrix}, \quad \text{where } \{i_1, i_2, \dots, i_{d'}\} \subseteq \{1, 2, \dots, d\}.$$

Then, a linear weighting $[n_0 \ \mathbf{n}']$ is learned using least squares regression, where:

$$g(z) \approx -n_0 * z + \mathbf{n}'^\top B_{d'}(\mathbf{m}, I) \quad \text{where } \{\mathbf{n}' = 1 \times d' \text{ vector}\} \tag{12}$$

To achieve the desired optimization of approximating $g(z)$, we begin with a large enough $B(\mathbf{m}, I)$ obtained by sampling from a uniform grid of values for \mathbf{m}, I . We then follow an iterative approach, wherein at each iteration t , we greedily pick a basis function i_j that has the highest alignment to the current residual estimate of $g(z)$. This can be observed as an adaptation of the well-established orthogonal matching pursuit (OMP) framework. A more detailed description of this process is provided below in Algorithm 1. It is worth noting, changing the original basis set $B(\mathbf{m}, I)$ to $B'(\mathbf{m}, I)$, could result in the algorithm converging to a different minima (global minima in $B'(\mathbf{m}, I)$ could be different from global minima in $B(\mathbf{m}, I)$). However, if the basis sets are equivalent we observe similar performance across simulations (Fig SI-9).

Algorithm 1 OMP for finding smallest RNN

- 1: Select a grid of values \mathbf{z} .
 - 2: Create global basis set \mathbf{B} using uniformly sampled \mathbf{m}, I values.
 - 3: Initialize n weights using linear decay term only: $n_0 = -(\mathbf{z}^\top \mathbf{z})^{-1} \mathbf{z}^\top g(\mathbf{z})$.
 - 4: Initialize residual: $r_0 = g(\mathbf{z}) - n_0 * (-\mathbf{z})$
 - 5: At each iteration t :
 1. Find basis vector with highest correlation with residual: $i_t = \arg \max_i \|\mathbf{B}_i^\top \mathbf{r}_{t-1}\|$
 2. Add new entry to the solution basis, $B_t \leftarrow \mathbf{B}_{i_t}$
 3. Solve to find new linear weights \mathbf{n}'_t using Eqn 9
 4. Compute the updated residual: $r_t = g(\mathbf{z}) - \mathbf{n}'_t^\top B_t$
 5. Check for termination based on a predefined sparsity threshold $d' = \text{len}(B_t)$
-

In Fig 3 we apply this method to a simulated 1D ODE, with two stable fixed points and one unstable fixed point. The first row shows the greedily-added basis functions, multiplied by their corresponding learned linear weightings. The bottom row shows their linear combination against the true underlying ODE. Through this iterative process, we observe with just 5 neurons our network almost perfectly reconstructs the target ODE.

It is worth noting, previous work (e.g., Luo et al. (2023); Valente et al. (2022)) have similar dynamics which are learned using BPTT with much larger networks (typically 512 neurons). Our method instead provides an empirical framework to find the minimum number of neurons needed to fit dynamics within estimated margins of error. Furthermore, we believe this could be used to provide insights on hyper-parameter values (such as number of neurons) for neural ODE models or other artificial networks.

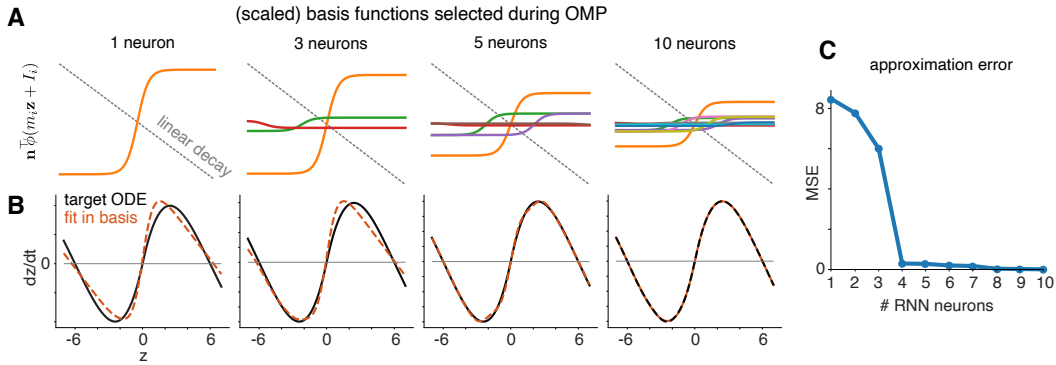


Figure 3: Finding the smallest RNN for a particular nonlinear dynamical system using orthogonal matching pursuit (OMP). (A) Scaled basis functions selected after 1, 3, 5, and 10 iterations of OMP, along with the linear decay term $-x$ for an example ODE (shown below). (B) Target ODE (black) and RNN fit after each step of OMP. (C) Mean squared error (MSE) between target ODE and RNN approximation as a function of the number of RNN neurons added by OMP.

5 NEW INSIGHTS INTO THE ROLE OF INPUT DYNAMICS

In Sec. 3, we demonstrated the importance of the presence of inputs in basis functions, $B(\mathbf{m}, I) = \phi(\mathbf{m}\mathbf{z} + I\mathbf{v}(t))$. Now, we highlight the influence of the type of inputs (constant or time-varying), in representing arbitrary ODEs. Specifically, our framework so far shows how autonomous ODEs ($g(\mathbf{z})$) are embedded via constant filtered inputs represented as $\mathbf{v} = 1$, that do not evolve over time. Here we extend our framework to embed non-autonomous ODEs ($g(\mathbf{z}, t)$) by introducing a dynamical system that governs the evolution of $\mathbf{v}(t)$.

Recent work has suggested an identifiability issue in uncovering underlying low-dimensional dynamics from high-dimensional neural activity, however the role inputs play in this hasn't been explored (Turner et al., 2021; Langdon & Engel, 2022; Liu et al., 2023; Qian et al., 2024). Furthermore, previous work on time varying inputs (Rajan et al., 2016; Remington et al., 2018; Galgali et al., 2023a) has focused primarily on whether observed trajectories were *input driven* or *dynamics driven*. We note here that this latter category can be subdivided into cases where the dynamics themselves are fixed in time or fluctuating due to inputs.

In Fig. 4 we illustrate using our framework to train low-rank RNNs that produce an identical trajectories (blue, red lines in the bottom row) through vastly different dynamical systems (quiver plots in bottom row). In all cases shown, the input dimension I is orthogonal to the dynamics subspace \mathbf{m} . Specifically, we demonstrate the following cases:

1. Autonomous ODE: Following the general treatment in Sec. 3 above, we embed an ODE of the form $\dot{\mathbf{z}} = g(\mathbf{z})$. The quiver plot (bottom row of panel A) represents the autonomous ODE flow-field illustrated through arrows of the same length across time, for each value of \mathbf{z} . Note, this embedding is achieved through inputs that are fixed in time ($\mathbf{v} = 1$). Additionally in the bottom row of panel A, the true trajectory (blue - computed using Euler integration), and the low-rank RNN (red - trained using Eqn 9), both start at the unstable fixed point ($\mathbf{z} = -6$), and eventually converge to the stable fixed point ($\mathbf{z} = +6$). The almost perfect overlap indicates the efficacy of our method.

2. Non-Autonomous ODE: In panels B,C,D we embed *time-varying* dynamics of various kinds into different low-rank RNNs. Our training objective was to create time-varying flow fields that produce a trajectory identical to the autonomous ODE case. The existence of time-varying dynamics can be observed by noting arrows of different lengths across time bins (i.e each row of quiver plot).

We first discuss how to embed such dynamics into the low-rank RNN. Intuitively, because the dynamic being approximated represents a different function over time, the basis functions also need to evolve in time. To achieve this embedding, we modeled inputs $\mathbf{v}(t)$ with an exponential decay given by $\dot{\mathbf{v}} = -\mathbf{v}$. This decay results in time-varying basis functions, as different $\mathbf{v}(t)$ values are computed at each Euler time-step when defining $\phi(\mathbf{m}\mathbf{z} + I\mathbf{v}(t))$.

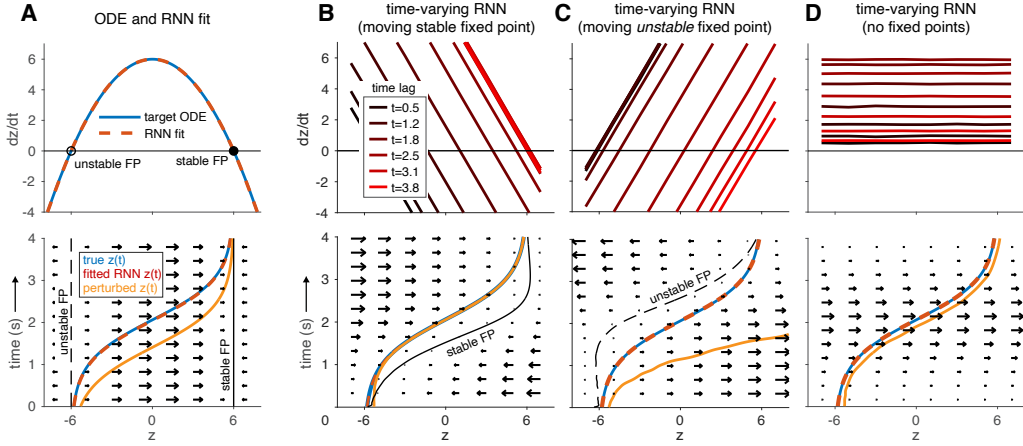


Figure 4: Creating indistinguishable time-varying dynamical systems with time-varying inputs. We show four different time-varying dynamical systems that give rise to the same (blue) target trajectory. (A) Top: we defined a target ODE defined by an inverted quadratic function (top), then embedded into an RNN with constant input (following the methods in Sec. 3). Bottom: we then simulated a trajectory that starts just right of the unstable fixed point and converges to the stable fixed point. Here the flow field dynamics do not vary in time. A perturbed input into the RNN (orange) follows the same trajectory, but shifted downward (earlier) in time. (B) We trained an RNN to produce a dynamic flow field using time varying basis functions, whose offsets shifted in time after clamping on an input u at time zero. Here we set the target to be a time-varying linear dynamical system with a single stable fixed point that moved from left to right. Note that the RNN latent (red) still follows the target trajectory (blue). However, the same perturbation shown in A now converges back to the target trajectory. (C) Network trained to produce the same target trajectory using a moving *unstable* fixed point. (D) Network trained to produce the same target trajectory using no fixed points. Note however that the trajectory arising from a perturbed initial point (yellow) varies wildly across these models.

Below, we expand on the specific dynamical system governing ODEs that can be approximated using such time-varying basis functions.

1. **Moving fixed points:** As already highlighted, the dynamical system of the target ODE is of the form $\dot{\mathbf{z}} = g(\mathbf{z}, t)$. Panels B, C present specific cases, where this dynamic represents an underlying flow-field which arises due to the diffusion of a single stable or unstable fixed point.

In other words, our target ODE represents the trajectory of a moving fixed point, modelled through a linear dynamic term in \mathbf{z} -

$$\dot{\mathbf{z}} = g(\mathbf{z}(t')) - \alpha * (\mathbf{z}' - \mathbf{z}(t')) - \mathbf{z}' \quad (13)$$

The above equation clearly highlights the systems' state depends on both $\{\mathbf{z}', t'\}$, representing a coarse spacing and a corresponding Euler time bin respectively. First, the term $\alpha * (\mathbf{z}' - \mathbf{z}(t'))$ introduces a linear time-varying correction which moves the fixed point of this system \mathbf{z}' to $\mathbf{z}(t')$ with a rate α , as shown in the top rows. Second, α must be positive for panel B (to move a single *stable* fixed point), and negative for panel C (to move a single *unstable* fixed point). Third, while the fixed point dynamic described above is linear, the system still evolves non-linearly due to the function g , as shown by the quiver plots. Lastly, in the absence of these dynamics the system decays to the fixed point defined by \mathbf{z}' .

2. **No fixed points:** Similar to the moving fixed point case, we can define a system with no fixed points during the movement from -6 to +6. In this case, the target ODE is defined by the non-linear evolution of $\mathbf{z}(t)$ with a time-invariant shift given as

$$\dot{\mathbf{z}} = g(\mathbf{z}(t')) - \mathbf{z}' \quad (14)$$

In the bottom row of panels B,C,D the true trajectory (blue) and RNN approximated trajectory (red) overlap. Critically, they are all identical, and in fact match the trajectories observed in the bottom row

of panel A. However, as discussed above, they all represent dramatically different target flow-fields, also showcased via their quiver plots.

Our results provide insight into how non-autonomous dynamics can be embedded into low-rank RNNs through time-varying inputs. It is worth noting that most current methods typically interpret low-dimensional dynamics post-training. One specific method that has gained popularity is the zero-finding method, which relies on finding fixed points (Sussillo & Barak, 2013; Smith et al., 2021). Our discussion on non-autonomous dynamics suggests, how similar trajectories can be observed in the presence of dynamical fixed points/ no fixed points at all. This presents a possible failure mode for such techniques. Additionally, we consider the effects of perturbations in the initial point (orange line in bottom row) for these different systems. As observed, while the learned RNN trajectory (black) is identical across all panels, small perturbations in the initial point lead to wildly different trajectories in different models, validating that observations of fixed trajectories are generally not sufficient to uniquely identify the underlying dynamical system (Galgali et al., 2023b).

6 COMPARISON WITH BPTT FOR NEUROSCIENCE TASKS

Finally, we apply our framework on two neuroscience inspired tasks (Wong & Wang, 2006; Sussillo & Barak, 2013; Luo et al., 2023) and compare our networks against RNN models trained with backprop-through time. Specifically, we implement:

1. **3-bit flip-flop task:** The network receives a series of bits (-1 or +1) in 3 registers, and must store the polarity of the most recent bit in each register (Sussillo & Barak, 2013).
2. **Binary decision-making:** Following previous literature, we model a sensory evidence accumulation task using bi-stable attractors (Wong & Wang, 2006). Sensory inputs drive the system from an unstable fixed point towards one of two stable fixed points, each associated with a different choice (see Appendix B for details).

In Sec. 4, we find the smallest low-rank ($r = 1$) network ($N = 10$ neurons) that almost perfectly fits a bi-stable attractor ODE. Here, we compare our model against networks of the same size (and rank) trained using BPTT. As shown, our method provides a closed form solution in one step, as compared to networks trained with BPTT which take an order of one/two more magnitudes to converge. In Fig. 5, panels B,C depict loss curves across a wide range of RNN models trained with BPTT. Consistent with previous findings we observe lower training loss for larger networks, although they take longer to converge. Additionally, low-rank networks ($r = 1$, panel C) have comparable performance for tasks with lower dimensionality. Second, our method qualitatively has better reconstruction of test trajectories (panel A). More importantly, our model significantly outperforms networks (order of magnitude lower test mean-squared error) of the same size (and rank) on a set of test target trajectories (panel D), thereby proving the efficacy of our method.

7 DISCUSSION

In this paper, we present an alternative view on low-rank RNNs that emphasizes interpretability and highlights the representational capacity of such networks. The focus of our work lies in defining a randomized basis which is used to embed an arbitrary non-linear dynamical system. We demonstrate that inputs are essential for capturing odd-symmetric functions through theoretical and empirical evidence. This extends previous work (Valente et al., 2022; Dubreuil et al., 2022; Beiran et al., 2021) and offers clarifying insights into when such models behave as universal function approximators. While previous work discusses universal approximation (Beiran et al., 2021) for such networks, we believe we're the first to provide a geometric basis function interpretation.

Furthermore, our formulation allows learning the parameters of this RNN in closed form with regression. By directly modeling the low-dimensional activity and transforming to neural activity space via a fixed linear projection, we reduce the number of parameters needed to be learnt. We achieve this by presenting an NEF approach (Eliasmith & Anderson, 2003) to train low-rank RNNs (a result also highlighted in (Beiran et al., 2021)). Our novelty lies in overcoming gradient-based training issues (in cases with known/estimated ODEs), similar to vector-field regression or teacher forcing algorithms (Heinonen et al., 2018; Bhat et al., 2020; Hess et al., 2023), with the added advantage of

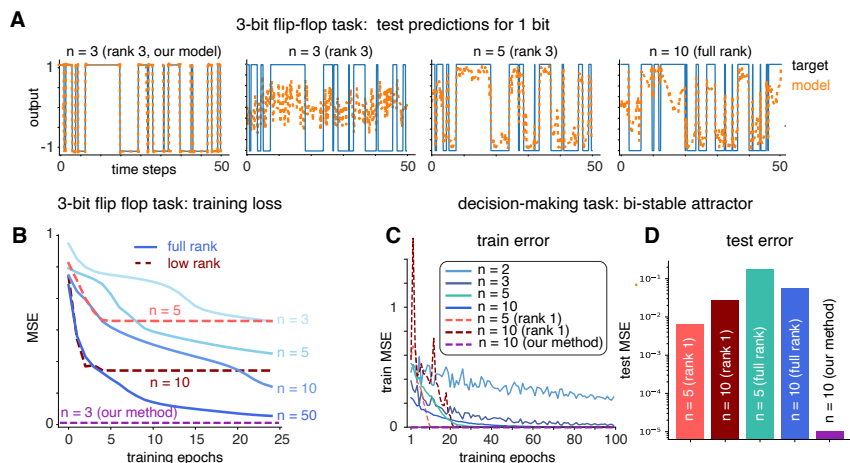


Figure 5: Comparisons to RNNs trained using backprop-through-time (BPTT) for neuroscience inspired tasks. (A) Target and trained RNN model outputs for one bit in the “3-bit flip-flop task”. Our model (left) achieves near perfect accuracy using only 3 neurons and a rank-3 weight matrix; low rank and full rank networks trained using BPTT do not achieve nearly the same level of accuracy. (B) Training loss as a function of number of training epochs for different networks. (Our network, which is trained in one step using least-squares regression is shown in purple for comparison). (C,D) Train and test error for RNNs trained to perform a binary decision-making task using bi-stable attractor dynamics (Wong & Wang, 2006; Luo et al., 2023).

not being stochastic across runs and requiring lower compute resources. Additionally, we directly provide an intuition on the role each neuron plays in the low-rank RNN. Our framework can thus be used as an alternative to task-training in neuroscience, to model novel behavioral tasks. Another exciting finding of our work is using OMP to approximate the smallest RNN (from a basis set), which could be used to drive insights on hyper-parameter values for such models. Together, this presents a promising future direction for studying how perturbing connectivity relates to unstudied behavioral outputs, or guiding experimentalists on capturing neurons with characteristic neural profiles (using OMP) for specific tasks.

We also present novel findings on the influence of input driven dynamics. Specifically, we directly link how non-autonomous ODEs can be embedded in low-rank RNNs through time-varying basis functions. Empirically, we demonstrate that identical trajectories can be generated from trajectories of moving fixed points, no fixed points or stationary target ODEs. The presence of dynamics in fixed points suggests a potential failure mode in current methods for interpreting such networks’ dynamics (Sussillo & Barak, 2013; Smith et al., 2021). Furthermore, we link the RNN connectivity to these target ODEs through dynamics along the input dimension. A potential future direction would be to guide causal perturbation experiments needed to uncover such dynamics. Additionally, although not explored here, the conversion of non-autonomous dynamics to autonomous dynamics could play a critical role in neuroscientific insight. Lastly, we prove the efficacy of our method by applying it to various neuroscience inspired tasks. We note our method outperforms models of similar size/rank trained with BPTT.

We conclude by discussing some limitations of our work. Our method relies on knowing (or estimating via finite differencing methods) the underlying latent dynamic. Additionally, the complexity of our framework lies in defining or estimating this underlying ODE. While in Sec. 5 we provide instances of embedding non-autonomous ODEs, arguably extending this to other higher order systems could be tricky. This might be especially useful while modeling multi-region brain interactions, where the state of the target ODE depends on another complex dynamical system as well. However, overall we believe the new insights provided by our framework outweighs its limitations and provides an exciting set of future directions.

REFERENCES

- 540
541
542 Larry F Abbott, Brian DePasquale, and Raoul-Martin Memmesheimer. Building functional networks of spiking
543 model neurons. *Nature neuroscience*, 19(3):350–355, 2016.
- 544 Alireza Alemi, Christian Machens, Sophie Deneve, and Jean-Jacques Slotine. Learning nonlinear dynamics in
545 efficient, balanced spiking networks using local plasticity rules. In *Proceedings of the AAAI conference on*
546 *artificial intelligence*, volume 32, 2018.
- 547 Omri Barak. Recurrent neural networks as versatile tools of neuroscience research. *Current opinion in*
548 *neurobiology*, 46:1–6, 2017.
- 549
550 Omri Barak and Sandro Romani. Mapping low-dimensional dynamics to high-dimensional neural activity: A
551 derivation of the ring model from the neural engineering framework. *Neural Computation*, 33(3):827–852,
552 2021.
- 553 Manuel Beiran, Alexis Dubreuil, Adrian Valente, Francesca Mastrogiuseppe, and Srdjan Ostojic. Shaping
554 dynamics with multiple populations in low-rank recurrent networks. *Neural Computation*, 33(6):1572–1615,
555 2021.
- 556 Harish S Bhat, Majerle Reeves, and Ramin Raziperchikolaei. Estimating vector fields from noisy time series. In
557 *2020 54th Asilomar Conference on Signals, Systems, and Computers*, pp. 599–606. IEEE, 2020.
- 558
559 Martin Boerlin, Christian K. Machens, and Sophie Denève. Predictive coding of dynamical variables in balanced
560 spiking networks. *PLoS Comput Biol*, 9(11):e1003258, 11 2013. doi: 10.1371/journal.pcbi.1003258. URL
561 <http://dx.doi.org/10.1371%2Fjournal.pcbi.1003258>
- 562 Ricky TQ Chen, Yulia Rubanova, Jesse Bettencourt, and David K Duvenaud. Neural ordinary differential
563 equations. *Advances in neural information processing systems*, 31, 2018.
- 564
565 Brian DePasquale, Christopher J. Cueva, Kanaka Rajan, G. Sean Escola, and L. F. Abbott. full-force: A
566 target-based method for training recurrent networks. *PLOS ONE*, 13(2):1–18, 02 2018. doi: 10.1371/journal.
567 pone.0191527. URL <https://doi.org/10.1371/journal.pone.0191527>
- 568 Alexis Dubreuil, Adrian Valente, Manuel Beiran, Francesca Mastrogiuseppe, and Srdjan Ostojic. The role of
569 population structure in computations through neural dynamics. *Nature neuroscience*, 25(6):783–794, 2022.
- 570 Lea Duncker and Maneesh Sahani. Dynamics on the manifold: Identifying computational dynamical activity
571 from neural population recordings. *Current opinion in neurobiology*, 70:163–170, 2021.
- 572
573 Chris Eliasmith and Charles H Anderson. *Neural engineering: Computation, representation, and dynamics in*
574 *neurobiological systems*. MIT press, 2003.
- 575 Aniruddh R Galgali, Maneesh Sahani, and Valerio Mante. Residual dynamics resolves recurrent contributions to
576 neural computation. *Nature Neuroscience*, 26(2):326–338, 2023a.
- 577
578 Aniruddh R Galgali, Maneesh Sahani, and Valerio Mante. Residual dynamics resolves recurrent contributions to
579 neural computation. *Nature Neuroscience*, 26(2):326–338, 2023b.
- 580 Markus Heinonen, Cagatay Yildiz, Henrik Mannerström, Jukka Intosalmi, and Harri Lähdesmäki. Learning
581 unknown ode models with gaussian processes. In *International conference on machine learning*, pp. 1959–
582 1968. PMLR, 2018.
- 583
584 Florian Hess, Zahra Monfared, Manuel Brenner, and Daniel Durstewitz. Generalized teacher forcing for learning
585 chaotic dynamics. *arXiv preprint arXiv:2306.04406*, 2023.
- 586
587 Herbert Jaeger. The “echo state” approach to analysing and training recurrent neural networks. *Bonn, Germany:*
German National Research Center for Information Technology GMD Technical Report, 148:34, 2001.
- 588
589 Ingmar Kanitscheider and Ila Fiete. Training recurrent networks to generate hypotheses about how the brain
590 solves hard navigation problems. *Advances in Neural Information Processing Systems*, 30, 2017.
- 591
592 Christopher Langdon and Tatiana A Engel. Latent circuit inference from heterogeneous neural responses during
593 cognitive tasks. *BioRxiv*, pp. 2022–01, 2022.
- 594
595 Timothy P Lillicrap and Adam Santoro. Backpropagation through time and the brain. *Current opinion in*
neurobiology, 55:82–89, 2019.

- 594 Yuhan Helena Liu, Aristide Baratin, Jonathan Cornford, Stefan Mihalas, Eric Shea-Brown, and Guillaume Lajoie.
595 How connectivity structure shapes rich and lazy learning in neural circuits. *arXiv preprint arXiv:2310.08513*,
596 2023.
- 597 Mantas Lukoševičius and Herbert Jaeger. Reservoir computing approaches to recurrent neural network training.
598 *Computer science review*, 3(3):127–149, 2009.
- 600 Thomas Zhihao Luo, Timothy Doyeon Kim, Diksha Gupta, Adrian G Bondy, Charles D Kopec, Verity A Elliot,
601 Brian DePasquale, and Carlos D Brody. Transitions in dynamical regime and neural mode underlie perceptual
602 decision-making. *bioRxiv*, pp. 2023–10, 2023.
- 603 Wolfgang Maass, Thomas Natschläger, and Henry Markram. Real-time computing without stable states: A new
604 framework for neural computation based on perturbations. *Neural Computation*, 14:2531–2560, 2002.
- 605 Valerio Mante, David Sussillo, Krishna V Shenoy, and William T Newsome. Context-dependent computation by
606 recurrent dynamics in prefrontal cortex. *Nature*, 503(7474):78–84, 2013.
- 607 Francesca Mastrogiuseppe and Srdjan Ostojic. Linking connectivity, dynamics, and computations in low-rank
608 recurrent neural networks. *Neuron*, 99(3):609–623, 2018.
- 610 Paul Miller, Carlos D Brody, Ranulfo Romo, and Xiao-Jing Wang. A recurrent network model of somatosensory
611 parametric working memory in the prefrontal cortex. *Cerebral Cortex*, 13(11):1208–1218, 2003.
- 612 Matthijs Pals, A Erdem Sagtekin, Felix Pei, Manuel Gloeckler, and Jakob H Macke. Inferring stochastic low-rank
613 recurrent neural networks from neural data. *arxiv [cs. lg]*, 2024.
- 614 Barak A Pearlmutter. Dynamic recurrent neural networks. 1990.
- 616 Arthur Pellegrino, N Alex Cayco Gajic, and Angus Chadwick. Low tensor rank learning of neural dynamics.
617 *Advances in Neural Information Processing Systems*, 36:11674–11702, 2023.
- 618 Eli Pollock and Mehrdad Jazayeri. Engineering recurrent neural networks from task-relevant manifolds and
619 dynamics. *PLoS computational biology*, 16(8):e1008128, 2020.
- 621 William Qian, Jacob A Zavatore-Veth, Benjamin S Ruben, and Cengiz Pehlevan. Partial observation can induce
622 mechanistic mismatches in data-constrained models of neural dynamics. *bioRxiv*, pp. 2024–05, 2024.
- 623 Kanaka Rajan, Christopher D Harvey, and David W Tank. Recurrent network models of sequence generation
624 and memory. *Neuron*, 90(1):128–142, 2016.
- 625 Evan D Remington, Seth W Egger, Devika Narain, Jing Wang, and Mehrdad Jazayeri. A dynamical systems
626 perspective on flexible motor timing. *Trends in cognitive sciences*, 22(10):938–952, 2018.
- 627 R. Schaeffer, M. Khona, L. Meshulam, International Brain Laboratory, and Ila R. Fiete. Reverse-engineering
628 recurrent neural network solutions to a hierarchical inference task for mice. *bioRxiv*, pp. 2020–06, 2020.
- 630 Friedrich Schuessler, Francesca Mastrogiuseppe, Alexis Dubreuil, Srdjan Ostojic, and Omri Barak. The interplay
631 between randomness and structure during learning in rnns. *Advances in neural information processing
632 systems*, 33:13352–13362, 2020.
- 633 Jimmy Smith, Scott Linderman, and David Sussillo. Reverse engineering recurrent neural networks with jacobian
634 switching linear dynamical systems. *Advances in Neural Information Processing Systems*, 34:16700–16713,
635 2021.
- 636 Terrence C Stewart. A technical overview of the neural engineering framework. *University of Waterloo*, 110,
637 2012.
- 638 David Sussillo. Neural circuits as computational dynamical systems. *Current opinion in neurobiology*, 25:
639 156–163, 2014.
- 641 David Sussillo and L. F. Abbott. Generating coherent patterns of activity from chaotic neural networks. *Neuron*,
642 63(4):544–557, Aug 2009. doi: 10.1016/j.neuron.2009.07.018. URL [http://dx.doi.org/10.1016/
643 j.neuron.2009.07.018](http://dx.doi.org/10.1016/j.neuron.2009.07.018)
- 644 David Sussillo and Omri Barak. Opening the black box: low-dimensional dynamics in high-dimensional
645 recurrent neural networks. *Neural computation*, 25(3):626–649, 2013.
- 646 Elia Turner, Kabir V Dabholkar, and Omri Barak. Charting and navigating the space of solutions for recurrent
647 neural networks. *Advances in Neural Information Processing Systems*, 34:25320–25333, 2021.

648 Adrian Valente, Jonathan W Pillow, and Srdjan Ostojic. Extracting computational mechanisms from neural data
649 using low-rank rnns. *Advances in Neural Information Processing Systems*, 35:24072–24086, 2022.
650
651 Alex H Williams, Erin Kunz, Simon Kornblith, and Scott Linderman. Generalized shape metrics on neural
652 representations. *Advances in Neural Information Processing Systems*, 34:4738–4750, 2021.
653 Kong-Fatt Wong and Xiao-Jing Wang. A recurrent network mechanism of time integration in perceptual
654 decisions. *Journal of Neuroscience*, 26(4):1314–1328, 2006.
655
656
657
658
659
660
661
662
663
664
665
666
667
668
669
670
671
672
673
674
675
676
677
678
679
680
681
682
683
684
685
686
687
688
689
690
691
692
693
694
695
696
697
698
699
700
701